Refinements in High-Reynolds Number Shock-Tunnel Technology

ROY SCOTT HICKMAN* AND JAMES B. KYSER†
McDonnell Douglas Aerophysics Laboratory, El Segundo, Calif.

The performance of a high-pressure (30,000 psi) shock tunnel is analyzed and compared to the measured performance of the McDonnell Douglas Aerophysics Laboratory Hypervelocity Shock Tunnel. It is shown that real-gas effects in the helium driver gas increase the shock Mach number for interface tailoring. Data and analysis for helium, nitrogen mixtures driving air exhibit similar trends but differ slightly in magnitude. The opening characteristics of thick diaphragms are analyzed and reasonable agreement is shown to exist between prediction and actual diaphragm behavior. The effects on shock-tunnel behavior are analyzed for a large nozzle-throat to driven-tube area ratio and significant loss of both stagnation pressure and enthalpy is shown to exist. For large throats the available test time is seen to be reduced severely for high-enthalpy cases.

Nomenclature

A = area
a = sound speed
B = second virial coefficient
C = third virial coefficient
C_p = specific heat at constant pressure
C_V = specific heat at constant volume
D = diameter
H = petal height
h = specific enthalpy
I = moment of inertia
L = length of buffer
M = Mach number
M_1 = moment due to pressure differential
M_2 = moment due to plastic stress at hingeline
n = number of petals
P = pressure
R_o = universal gas constant
S = strength factor (Eq. 11)
S_{LIMIT} = maximum value of S that will allow the diaphragm to open completely
T = temperature
t = time
t_b = characteristic time of buffer
t_d = characteristic time of diaphragm opening
u = velocity
V = specific molar volume
w = petal base width
x = distance
α = fraction of petal untorn at hingeline
γ = ratio of specific heats
δ = petal thickness
θ = petal opening angle
ρ = density
σ = plastic (ultimate) stress at hingeline
τ = nondimensional time
τ^* = time required for reflected shock to traverse buffer
τ_m = nondimensional time of impact
ϕ = energy integral (Eq. 12)

Superscripts

$*$ = critical value
$(\cdot)$ = differentiated with respect to t
$()'$ = differentiated with respect to τ

Subscripts

A,B,C = regions defined in Fig. 6
i = initial buffer section value
r = reflected shock wave
s = incident shock wave
1–6 = regions in shock tube (Fig. 2)

Introduction

RECENT interest in lifting and maneuvering re-entry vehicles, both manned and unmanned, has produced a need for high-Reynolds number hypersonic test facilities. This need comes about because of the requirement to simulate hypersonic flight conditions where the vehicle boundary layer is fully turbulent. Facilities which have the possibility of providing the essential test environment are: the blowdown facilities, in which the test gas is heated by a furnace; the hotshot, in which the test gas is heated by a spark; and the shock tunnel, in which the test gas is heated by a shock wave. The first two types of facilities have certain limitations in pressure, temperature, mass-flow rate, or gas composition, most of which can be overcome in the shock tunnel. The shock tunnel, when specialized for high-pressure operation, appears to be the most suitable facility for high-Reynolds number hypersonic testing where test objectives can be met during its short (up to 5 msec) run duration.

One of the current high-pressure shock tunnels is the Hypervelocity Shock Tunnel at the McDonnell Douglas Aerophysics Lab. (MDAL) in El Segundo, Calif. It has a 22-ft-long driver tube with a 7-in. internal bore capable of being pressurized to 30,000 psi. Cold or heated helium or mixtures of helium and nitrogen can be used as a driver gas. The driven tube is 43 ft long and has an internal bore of 5.2 in. It is usually filled with air at a few hundred psi. Reservoir pressures in excess of 20,000 psi and Reynolds numbers in excess of 100 million/ft can be obtained.

With driver-gas pressures of the magnitude discussed above, meaningful calculations of the shock-tube processes, such as shock Mach number for interface tailoring, cannot be made without using a detailed equation of state. Deviation from the ideal equation of state is reflected in the compressibility factor, which becomes as large as 1.5 to 2.0 at these pressures.

The diaphragms used in the MDAL shock tunnel are commonly $\frac{1}{2}$ to $\frac{5}{8}$ in. thick, and their performance plays an important

Presented as Paper 72-996 at the AIAA 7th Aerodynamic Testing Conference, Palo Alto, Calif., September 13–15, 1972; submitted December 1, 1972; revision received March 19, 1973. Work supported by the McDonnell Douglas Independent Research and Development Program.

Index categories: Supersonic and Hypersonic Flow; Nonsteady Aerodynamics.

* Consultant; also Associate Professor of Mechanical Engineering, University of California at Santa Barbara.

† Section Chief, Advance Projects. Member AIAA.

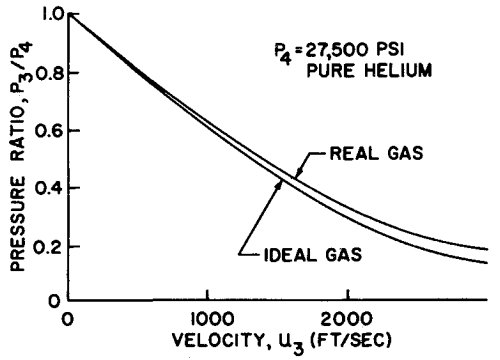

Fig. 1 Comparison of real-gas and ideal-gas unsteady expansion of helium.

role on the over-all performance of the shock tunnel. This paper reports the results of analytical and experimental studies to develop a satisfactory thick-diaphragm design for this facility. In addition, the effects on shock-tunnel performance of certain characteristics of high-Reynolds number shock tunnels, such as a large nozzle throat in the shock tube endwall and a massive diaphragm, are discussed.

High-Pressure Interface Tailoring

Tailored operation of a shock tube is achieved when the shock wave reflected from the driver-tube end wall passes through the interface without producing either reflected expansion or compression waves in the driven gas. For given ideal driver and driven gases at specified initial temperatures, tailored operation can be obtained at only one incident shock Mach number. The practical operation of a shock tunnel requires that the stagnation enthalpy of the flow be varied and tailored interface conditions be maintained. This is accomplished by heating the driver gas or by adding a high-molecular weight gas to the driver gas, which commonly is helium, to permit interface tailoring over a wide range of shock Mach numbers. Flagg[1] has performed extensive calculations for ideal gases and has obtained tailoring shock Mach number as a function of driver-gas to driven-gas sound-speed ratio. At high pressures, the behavior of the driver gas can deviate significantly from that of a perfect gas because density no longer varies with pressure in an ideal manner. Consequently, tailoring Mach number becomes a function of driver pressure as well as driver temperature and molecular weight.

The tailoring calculations presented in this paper use the virial equation of state

$$PV/R_o T = 1 + B/V + C/V^2 + \cdots \quad (1)$$

B and C are the second and third virial coefficients and must be obtained from a specified potential interaction model. Throughout these calculations, the Lennard-Jones 6–12 values as listed by Hirschfelder et al.[2] are used. The air in the driven section is treated as an ideal gas for computation of the shock wave processes. This assumption is justified by the fact that the compressibility of the driven gas is always low compared to the relatively cold driver gas. Calculations by Lewis and Burgess[3] indicate that, for initial driven-gas pressures of 200 psi, the compressibility of the air behind the reflected shock wave does not exceed 1.09 for incident shock Mach numbers less than 4.5. The values of pressure, velocity, and sound speed behind the incident shock wave are shown to be close to those for an ideal gas. As this discussion is directed toward high-Reynolds number hypersonic testing, incident shock Mach numbers higher than 4.5 are of relatively little interest.

For an unsteady one-dimensional expansion of a continuum fluid, the momentum equation can be written as $du = -dP/\rho a$. This equation, coupled with the equation of state and a process specification, allows the calculation of the behavior of driver gases in shock tubes.[4] For an isentropic expansion, the equation $dT = T\,\partial V/\partial T|_P\, dP/C_P$ is known to hold. To perform an expansion calculation, the value of $T\,\partial V/\partial T|_P$ is required in terms of the virial coefficients. This is easily found from Eq. (1) to be

$$T\left.\frac{\partial V}{\partial T}\right|_P = \frac{V + (R_o T/P)[(T/V)\,dB/dT + (T/V^2)\,dC/dT]}{1 + (R_o T/PV^2)(B + 2C/V)} \quad (2)$$

Expressions for C_p, C_v, h, and a in terms of the virial coefficients are available in Hirschfelder et al.[2] The above equations comprise a sufficient set to calculate the behavior of high-pressure single-component gas in an unsteady expansion, providing the zero-pressure thermodynamic behavior of the gas is known. Since all of the expansions considered in this paper start near room temperature, C_p can be taken as the constant value $5/2\,R_o$.

Figure 1 is a plot of the pressure ratio across an unsteady expansion of helium starting at 27,500 psi vs the velocity produced by the expansion. As can be seen, for a specified pressure ratio, the real-gas behavior results in a higher value of velocity than for an ideal gas. The presence of small mole fractions of nitrogen in the driver gas complicates the calculation of the driver-gas virial coefficients. To include these effects, the procedure of Amdur and Mason[5] is used. In all calculations, the fourth virial coefficient was estimated but not used as it always provides less than a 1% contribution.

The numerical computation technique is a simple forward-step process. The driver gas is assumed to undergo an unsteady expansion with a small drop in pressure. The velocity change and thermal properties for each step are then calculated. For a set of driver conditions, a value of P_3 (refer to Fig. 2 for notation) which would be slightly above the tailored value is estimated. The unsteady calculation is stopped at this value of P_3, and the current values of u_3 and P_3 are stored for later use. At this point, the required values of incident shock Mach number and P_1 which will produce P_2 equal to P_3 and u_2 equal to u_3 are computed. Then the pressure P_5 generated by a stopping shock wave in the driven gas is computed from ideal-gas relationships. In the case of a shock tube with a nozzle throat in the end wall, the stopping shock reduces the velocity to the drift velocity required to achieve sonic flow in the nozzle throat. The pressure P_6 generated by a stopping shock in the driver gas is computed from real-gas relationships. If P_5 and P_6 are not equal, they are printed out along with current values of u_3, P_3, and shock Mach number, and the computer returns to the unsteady expansion. When a set of conditions is reached at which $P_5 = P_6$, the interface is tailored and the computer run is terminated. For the case of an area reduction at the diaphragm station, the properties across the steady expansion generated by the area reduction are computed and used in the calculations. A typical computation requires 30 sec on an IBM 360/75 computer.

The Mach number at which interface tailoring occurs, as a function of pressure for pure helium driving air, is shown in Fig. 3. The analytical curve shows that as P_4 increases the tailoring Mach number increases due to the effects of increasing compressibility. The predicted trends agree reasonably well with the

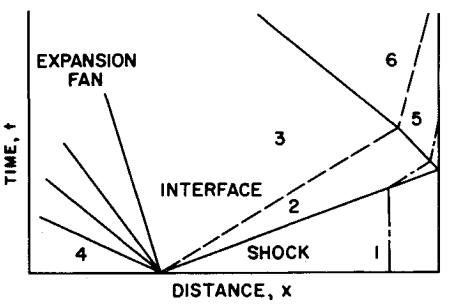

Fig. 2 $x-t$ diagram for tailored operation.

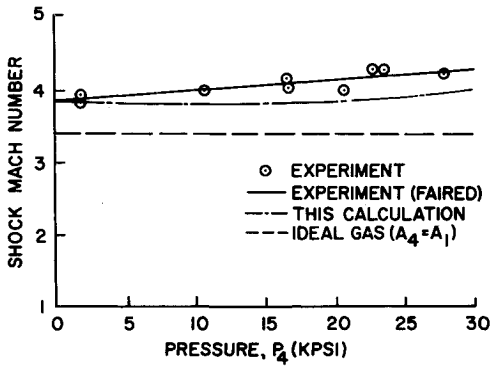

Fig. 3 Tailoring Mach number for helium driving air.

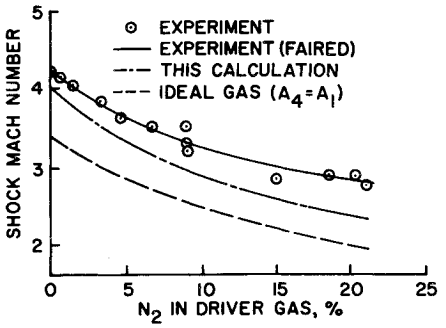

Fig. 4 Tailoring Mach number for helium, nitrogen mixtures driving air, $P_4 = 27{,}500$ psi.

experimental data, showing the tailoring Mach number to increase approximately linearly with pressure at all driver pressures investigated. Although these data correspond to both driver and driven gas nominally at room temperature, it should be noted that the temperature of the driver gas was actually 20°F higher than room temperature due to work of compression of helium. It is estimated this effect increases the tailoring Mach number by approximately 0.05. The ideal-gas curve in Fig. 3 is taken from Flagg[1] and is for constant area. Direct comparison with his results is difficult because, for the geometry of the MDAL shock tunnel, an unsteady expansion exists on either side of the area reduction. A more exact ideal-gas calculation[6] involving both the unsteady expansion and the 20°F driver temperature increase will agree with the low-pressure real-gas calculation tailoring Mach number to within 0.1.

Figure 4 is a plot of tailoring Mach number vs mole fraction of nitrogen for driver pressure ranging from 25,000 to 30,000 psi. Both calculation and experiment are for driver and driven gas nominally at room temperature. Both involve an area reduction corresponding to a diameter reduction of from 7.0 in. to 5.2 in. at the diaphragm station. Also shown is a curve for ideal-gas tailoring.[1] Figure 4 shows the real-gas calculations to be in reasonable agreement with measurements. Both the real-gas and the ideal-gas calculations are seen to exhibit the correct trend as gas composition is varied. Test conditions were varied by fixing the shock Mach number and adjusting the driver-gas composition until tailored operation was achieved; that is, until the reservoir-pressure trace was, on the average, invariant with time between the arrival of the incident shock and the arrival of the reflected expansion wave. As can be seen, measured shock Mach number for tailoring drops from a value of 4.25 with 100% helium to a value of 3.0 with 80% helium and 20% nitrogen.

Nozzle Throat Effects

The effects of a nozzle throat in the shock-tube end wall on shock-tube performance characteristics will be discussed in this section. This factor is particularly important to high-Reynolds number shock-tunnel operation because large nozzle throats are frequently employed to achieve increased Reynolds number at the sacrifice of Mach number. Nozzle effects are manifest in three forms: incomplete reflection of the incident shock wave, effect on interface tailoring, and rapid depletion of the test gas. These are the subjects of the following paragraphs.

It is observed that in an ideal gas the velocity change across any standing shock wave can be expressed as

$$\Delta u/a = [2/(\gamma+1)][M - 1/M] \quad (3)$$

where a is the upstream sound speed and M is the Mach number of the flowing gas. If Eq. (3) is applied successively to the incident shock wave and to the reflected shock wave, one obtains

$$M_2 - [M_5 a_5/a_2] = [M_r - 1/M_r]2/(\gamma+1) \quad (4)$$

Where M_r is the Mach number of the gas of region 2 relative to a standing reflected shock wave. This relative Mach number of the reflected shock wave M_r will determine the ratio of both enthalpy and pressure in region 5 to that in region 2. The value of M_2 is only a weak function of the incident shock strength, changing from 1.5 at $M_s = 2.0$ to 1.6 at $M_s = 4.5$. It is difficult to solve Eq. (4) explicitly for M_r because a_5/a_2 is a function of M_r.[4] The value of M_5 depends only upon the area ratio of the nozzle used in the shock tunnel and is the required drift Mach number obtained from simple one-dimensional nozzle calculations for the gas. To obtain Fig. 5, an intermediate solution to Eq. (4) for a fixed value of M_2 (corresponding to $M_s = 4.0$) is obtained by varying M_4 and computing M_5. Then, for a given nozzle area ratio M_5 is known and M_r can be found. The ratios h_5/h_2 and P_5/P_2 are then simply the Rankine Hugonoit equations

$$h_5/h_2 = [2\gamma M_r^2 - (\gamma-1)][(\gamma-1)M_r^2 + 2]/[(\gamma+1)M_r]^2 \quad (5)$$

and

$$P_5/P_2 = [2\gamma M_r^2 - (\gamma-1)]/(\gamma+1) \quad (6)$$

To obtain h_5/h_2 and P_5/P_2 for $A^* = 0$, M_5 is set equal to zero in Eq. (4) and the corresponding values are computed. The results of these calculations are shown in Fig. 5 for an incident shock Mach number of 4.

For a 2.6-in.-diam throat in a 5.2-in.-diam driven tube, where $A^*/A_5 = 0.25$, it is found that $P_5/P_{5(A^*=0)} = 0.83$, which implies a 17% loss of reflected pressure. Experimental values of pressure ratio obtained in the MDAL shock tunnel are shown in Fig. 5 and are seen to agree well with the computed values. A 9% reduction is seen to exist for the stagnation enthalpy. Although the effect of throat area on reflected pressure is of little consequence in computing stream properties (since reflected pressure is a measured quantity), a severe error can occur if the effect on stagnation enthalpy (which is a computed quantity) is not taken into account. The curves in Fig. 5 are not strong functions of Mach number since this effect is removed by normalizing with respect to values for $A^* = 0$.

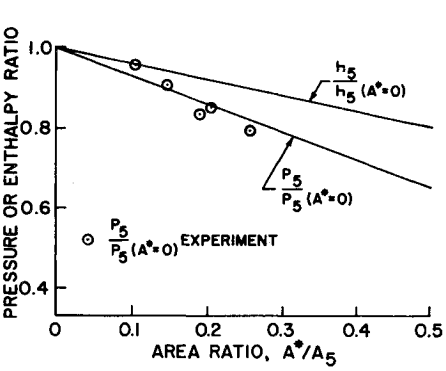

Fig. 5 Reflected pressure and enthalpy loss due to a nozzle throat in the end wall, $M_s = 4$.

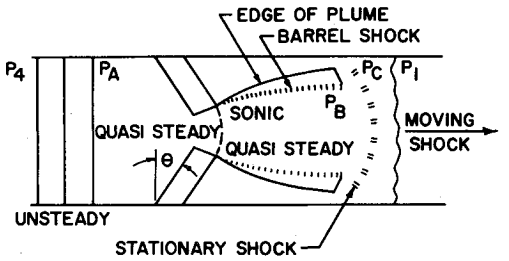

Fig. 6 Schematic diagram of flow during diaphragm opening.

Ideal-gas calculations were also undertaken to provide an estimate of the change in tailoring Mach number due to the presence of a nozzle in the end wall. No detectable change in tailoring Mach number is found to occur. This result arises because tailoring conditions depend primarily upon the sound-speed ratio across the driver-gas, driven-gas interface and not upon the final sound speed, pressure, or drift velocity in region 5. Since ideal-gas tailoring calculations were shown in Fig. 4 to predict trends correctly for the real-gas case, it is reasonable to assume that little effect on tailoring conditions due to a nozzle in the end wall will be observed in the real-gas case.

Ordinarily shock-tunnel test time is limited by the reflected expansion fan shown in Fig. 2. A large nozzle throat in the shock-tube end wall can have a serious effect on test duration because the high mass flow through the throat depletes the test gas. To demonstrate the effect of a large throat, a test duration requirement of 2 msec to establish steady flow and 5 msec to acquire data is arbitrarily assumed. Calculations[7] taking interface mixing into account show that a 43-ft-long room temperature driven tube will not provide enough gas to meet this test-duration requirement at temperatures higher than about 2500°R when a throat diameter of one-half the driven-tube diameter is used. Furthermore, at temperatures above about 4000°R, there will be barely sufficient gas for the 2 msec flow-establishment time. If the 4000°R test condition is achieved by preheating the driven tube to 1200°R and reducing the shock Mach number to 2.5, additional test gas will be processed and the quantity of gas will be adequate for the 2 msec flow establishment time plus 3 to 4 msec of steady flow. This suggests that serious consideration should be given to preheated driven tubes for high-Reynolds number testing.

Thick Diaphragm Behavior

Figure 6 shows a side view of a partially open diaphragm that is thick compared to its diameter and the assumed flow pattern through its petals. The diaphragm is assumed to be planar and θ is its angular displacement. In order to predict the pressure across the diaphragm, and hence to obtain the driving moment, an approximation to the gas process on each side of the diaphragm is necessary. In this analysis it is assumed that the projected area of the open space between the diaphragm petals is the sonic area for a quasi-steady expansion from conditions upstream of the nozzle formed by the petals. The flow on the upstream side of the diaphragm is then given by an unsteady expansion in the driver tube followed by a steady expansion through the diaphragm. The downstream flow is assumed to be composed initially of a plume from the projected open space expanding to the driven-tube area. A steady normal shock wave processes the gas that drives the moving principal shock down the driven section. As the diaphragm opens further, the strength of the steady normal shock in the tube decreases and the flow downstream of the shock must gradually accelerate. This model is consistent with the analyses of Russel[8] and White.[9]

The open area ratio of the diaphragm can be expressed as $A/A^* = 1/(1-\cos\theta)$. From the area ratio, the Mach number and pressure upstream and downstream of the diaphragm can be computed as a function of θ. The diaphragm petal is governed by the equation of motion

$$I\ddot{\theta} = M_1 - M_2 \tag{7}$$

where M_1 is the moment due to the pressure differential acting on it and M_2 is the moment due to plastic stress at its hinge line. M_1 and M_2 are given by

$$M_1 = (P_A - P_B)wH^2/6 \tag{8}$$

and

$$M_2 = \alpha(\sigma\delta/2)(\delta/2)w \tag{9}$$

It is assumed that the stress σ is constant and in tension over half the diaphragm thickness and in compression over the other half. The ultimate stress is used for σ since for most steel the ultimate strength and yield strength become equal for strain rates greater than 100 in./in./sec.[10] The strain rates in diaphragms used in this study commonly exceeded 300 in./in./sec. If the diaphragm has n petals and its diameter is D, the height of each petal is $(D/2)\cos(\pi/n)$. Then Eq. (7) can be written as

$$\frac{\cos(\pi/n)\rho\,\delta D}{4P_4}\ddot{\theta} = \left(\frac{P_A}{P_4} - \frac{P_B}{P_4}\right) - \frac{6\alpha\sigma\delta^2}{D^2P_4\cos^2(\pi/n)} \tag{10}$$

If the substitution $\tau = \frac{1}{2}\{[\rho\delta D\cos(\pi/n)]P_4\}^{1/2}\tau$ is made, Eq. (10) becomes

$$\theta'' = (P_A/P_4 - P_B/P_4) - S \tag{11}$$

where

$$S = \frac{6\alpha\sigma\delta^2}{D^2P_4\cos^2(\pi/n)}$$

and is not a function of θ or time, P_A/P_4 and P_B/P_4 are functions of θ, and $\theta' = d\theta/d\tau$. Equation (11) can be rewritten as

$$\phi = \frac{1}{2}\left(\frac{d\theta}{d\tau}\right)^2 + S\theta = \int_0^\theta \left(\frac{P_A}{P_4} - \frac{P_B}{P_4}\right)d\theta \tag{12}$$

where ϕ is an energy integral. It is assumed that the diaphragm starts from rest when $\theta = 0 = \tau$. The function within the brackets must be obtained numerically with the aid of one-dimensional nozzle tables, and the result is plotted in Fig. 7. As can be seen, the value of the energy integral ϕ can be obtained for any value of θ. For a diaphragm that opens completely and stops at $\theta = 90°$ without slapping the wall, ϕ must be equal to 1.104. From this, the optimum value of S is found to be 0.71. The optimum value of S is defined as that value of S for which the diaphragm opens fully but does not slap the wall.

The displacement vs time is shown in Fig. 8 for $S = 0.71$. The nondimensional time corresponding to the moment of impact, τ_m, is 6.23 for this case. It is clear that the distance traveled by the incident shock wave during the opening process must be small compared to the total driven-tube length. With shock Mach numbers near 4.0 in the MDAL shock tunnel, the 43-ft-long driven tube is adequately long, since the opening time for an optimum performance diaphragm is about 700 μsec and the shock travels only 2.8 ft. As will be discussed later, most practical diaphragms have a value of S of 0.3 or less and actually

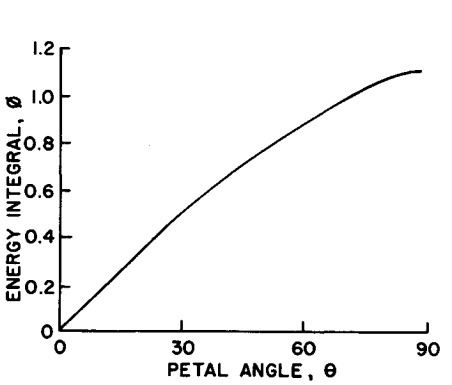

Fig. 7 Energy integral for diaphragm petal vs petal angle for helium driver gas.

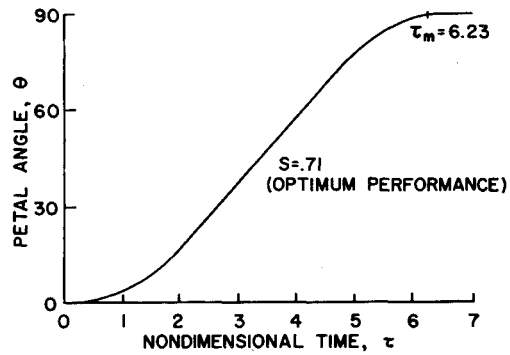

Fig. 8 Diaphragm petal opening amgle vs nondimensional time.

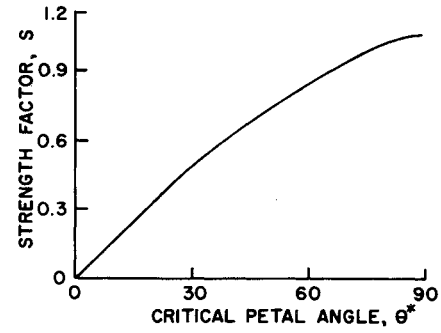

Fig. 9 Maximum petal strength factor for complete opening.

open in a much shorter time, consequently striking the wall with varying amounts of force.

This analysis has been developed for the case of a diaphragm with n petals. It was implied in the derivation that each petal could be treated as triangular in shape. These results are applicable to the downstream diaphragm in a double-diaphragm shock tube, as well as to the diaphragm in a single-diaphragm shock tube, provided that the upstream diaphragm opens most of the way before the downstream diaphragm ruptures. The eight-petal downstream-diaphragm configuration has been found useful to reduce tearing at the petal hingeline and thus reduce the incidence of petal loss.

It is common practice in high-pressure shock tubes to facilitate rupture of the diaphragm by operating with double diaphragms separated by a buffer region. The two diaphragms each will withstand half but not all of the differential pressure $P_4 - P_1$. The intermediate section, or buffer, between the diaphragms is maintained at a pressure P_i selected to prevent overloading of either diaphragm. Diaphragm rupture is initiated by venting P_i to the atmosphere and allowing the upstream diaphragm to rupture, causing the downstream diaphragm to be overloaded and consequently to rupture. The previous analysis of a single diaphragm will be modified in the following paragraphs to include the effects of the buffer. The results will then describe the behavior of the upstream diaphragm in a double-diaphragm shock tube. It will be assumed that the upstream diaphragm follows the model presented in the previous paragraphs with one exception. Instead of gas being supplied continuously to the driven tube, it will be assumed that the buffer is filled by the quasi-steady flow through the opening diaphragm.

The flow into the buffer region terminates when the shock generated at the downstream end of the buffer to stop the gas flow has traversed the length of the buffer section and arrived at the upstream diaphragm. The equations of motion are the same as previously developed except that the term $(P_A/P_4 - P_B/P_4)$ in Eq. (11) goes to zero when the reflected shock reaches the upstream diaphragm. Then, for complete opening, the kinetic energy of the diaphragm must equal the energy required to move the diaphragm petal through the remaining angle. With the pressure force term eliminated, the equation for the terminal angular rate is obtained

$$(\tfrac{1}{2}\theta'^2)_{\theta=\pi/2} = (S\theta + \tfrac{1}{2}\theta'^2)_{\theta=\theta^*} - S\pi/2 \tag{13}$$

where θ^* is the angle at which the buffer has "filled" and the flow into it terminates. If it is assumed that θ^* is known, the maximum allowable value of S which can be tolerated and which will allow the diaphragm to open completely (i.e. $\theta' = 0$ at $\pi/2$) is given by

$$S_{\text{LIMIT}} = (2/\pi)(\tfrac{1}{2}\theta'^2 + S\theta)_{\theta=\theta^*} \tag{14}$$

This value of S is plotted in Fig. 9 as a function of θ^*. If it is known when the flow stops, then the maximum value of S allowable to open the diaphragm can be obtained. In practice a value of S from 20 to 50% less than this limiting value has proven to be most successful.

To estimate the duration of gas flow into the buffer, the actual filling process for a buffer of length L must be analyzed. This is accomplished by computing the trajectory $(x-t)$ of the stopping shock wave which will terminate the flow when it reaches the upstream diaphragm. If the velocity of the shock is u_r, and it is assumed that the stopping shock starts moving from the downstream diaphragm immediately, (i.e., at $\tau = 0$), the shock will traverse the buffer in the time τ^* defined by

$$L = \int_0^{\tau^*} u_r\, dt \tag{15}$$

u_r is a function of the Mach number downstream of the diaphragm and is easily calculated. Substituting τ for t in Eq. (15) yields

$$\Sigma \frac{u_r}{a_4}\Delta\tau = \frac{2L}{a_4}\left(\frac{P_4}{\rho\delta D\cos\pi/n}\right)^{1/2} \tag{16}$$

If the substitutions $L/a_4 = t_b$ and

$$\frac{1}{2}\left(\frac{\rho\delta D\cos\pi/n}{P_4}\right)^{1/2} = t_d$$

are made, Eq. (16) becomes

$$\Sigma(u_r/a_4)\Delta\tau = t_b/t_d \tag{17}$$

The relative magnitudes of both t_b and t_d are 100 to 1000 μsec. Figure 10 gives the results of the filling calculations for pure helium, and can be used as follows: If S is known (say 0.6) and $t_b/t_d = 0.5$, then the flow into the buffer stops at $\theta^* = 79°$.

Several examples of diaphragm behavior calculations have been made and compared to observed behavior. Both fully opened and partially opened diaphragms were considered. Although little quantitative information is available regarding the fully opened diaphragms, indication of the petal speed at impact can be obtained from an inspection of the petal tip condition. During a recent series of tests, the dimensions of Table 1 Case A were used for the diaphragm.

These dimensions yield for the upstream diaphragm $S = 0.22$,

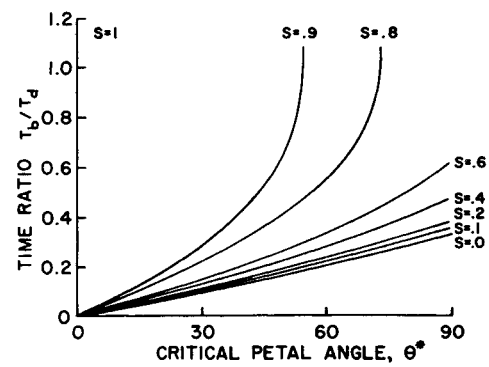

Fig. 10 Effect of buffer to diaphragm time ratio on petal angle at which inflow stops.

Table 1 Configuration of petals used for sample calculations

	Case A	Case B
D	7.5 in. equivalent upstream—square cross section 5.0 in. equivalent downstream	5.0 in. equivalent upstream 5.0 in. equivalent downstream
δ	0.625 in.	0.5 in.
Material	Stainless steel	Stainless steel
σ	84,000 psi	84,000 psi
P_4	27,000 psi	15,000 psi
α	0.8 upstream; 1.0 downstream	1.0 upstream; 1.0 downstream
L	3.75 in.	3.00 in.
a_4	3500 ft/sec	3500 ft/sec
n	4 petals on upstream 8 petals on downstream	4 petals on upstream diaphragm 4 petals on downstream diaphragm

$t_b = 0.089$ msec, and $t_d = 0.16$ msec. From Fig. 10 it is seen that the upstream diaphragm should hit the wall. To perform this calculation the actual buffer length has been used. However, an effective buffer length which is more representative of the actual length must be used since the reflected buffer shock does not have to travel the entire buffer length to reach the opening diaphragm petals. An iteration in which the buffer length is shortened by $(D/2)\cos\theta^*$ from the previous calculation is used to obtain a value of θ^* that is consistent with the nondimensional time ratio and the actual buffer length. This yields a value of $t_b/t_d = 0.163$. From Fig. 10 it is seen that the critical angle at which force stops is close to 44°. At this angle the nondimensional angular energy is, from Fig. 9, $\frac{1}{2}\theta'^2 = 0.55$. From Eq. (13) the nondimensional angular energy at $\theta = \pi/2$ is found to be 0.28. The computed angular rate is 5.5 rad/msec or the tip velocity is 1200 fps. It is desirable that the upstream diaphragms slap the tube wall with a velocity sufficient to straighten out any initial bulge. The value of S for the downstream diaphragm is 0.34. The computed tip velocity at full opening is 1280 fps. Both the upstream and downstream diaphragm behavior are borne out by experiment. It is evident that the upstream diaphragm strikes the wall with less impact than the downstream petals, as the downstream petals are more deformed from impact than the upstream petals.

As an example of incomplete opening, the diaphragm behavior of the upstream and downstream diaphragms shown in Table 1 Case B will be discussed. The value of S was 0.58, indicating that the downstream diaphragm should slap the wall. The apparent curvature and shape of the downstream petal does indeed exhibit this. The iterative calculations for the angular position at which the upstream petals should stop yields an angle of $\theta = 79°$. The average measured terminal angle is 60°. It must be recalled that the ultimate stress has been used throughout the calculations and constant compressive and tensile stresses were assumed over each half-diaphragm thickness. The moment required to overcome the petal curvature due to preloading has not been accounted for and might account for the discrepancy. Also, the petals are known to spring back slightly due to elastic behavior or to the reflected shock, which loads the petals in the opposite direction.

An experimental study of diaphragm performance was conducted to identify additional diaphragm characteristics. For reasons of economy, $\frac{1}{2}$-in. diaphragms and a driver pressure of 15,000 psi were used for one portion of the study, and additional results were obtained from observations of diaphragm behavior during routine tests conducted in the MDAL shock tunnel at pressures as high as 27,000 psi. Diaphragm performance was evaluated either by measuring the open area or by computing the effective driver pressure from the measured P_1 and shock speed and dividing this effective pressure by the measured driver pressure. The quotient is referred to as the diaphragm efficiency.

The results of the test with $\frac{1}{2}$-in. diaphragms were as follows: A long (1 diam) buffer configuration gave 16% less open area than the standard-length ($\frac{1}{2}$ diam) buffer. A square configuration gave an increase of 17%, and the high-pressure (groove depth 15% of diaphragm thickness) upstream diaphragm configuration gave an increase of 45%. The only real surprise in these results is the relatively poor performance of the long buffer configuration, probably caused by an excessively slow buffer dump rate. In all cases, the corresponding downstream diaphragm opened significantly better than the upstream one.

From these results, it is apparent that the upstream diaphragm should have a groove depth 15% of thickness and be designed to burst at a differential pressure as close to $P_4 - P_1$ as practical; the buffer section into which it breaks should have a square cross section. Earlier attempts to improve diaphragm performance by reducing the material thickness resulted in petal loss. Diaphragms which were able to withstand 80 to 90% of the differential pressure $P_4 - P_1$ were also the thinnest diaphragms that would withstand the reflected shock loads.

The observations of $\frac{5}{8}$-in. diaphragm behavior have produced refinements in technique that have given improved opening characteristics and virtually eliminated petal loss. These refinements are as follows:

a) A minimum elongation of 70% is specified for the types of stainless steel alloy and one type of carbon steel alloy which were used for diaphragms during these studies. The highest ductility material gave best performance; identical runs with diaphragms of differing ductility have shown that a 5% to 7% improvement in the diaphragm efficiency can be realized with a moderate increase in ductility. A side benefit is an observed reduction in the incidence of diaphragm petal loss.

b) The upstream diaphragm groove has been machined with a variable depth to give a more nearly constant stress. Near the edge of the diaphragm, where the stress is greatly reduced, the groove depth is increased. This permits the remaining metal to tear easily and facilitates the final steps in petal formation.

c) An orifice plate with a square opening has been placed just downstream of the buffer to form a fence to deflect the flow behind the reflected shock wave and prevent bending of the upstream petals in the reverse direction. The fence is designed to be just slightly higher than the fully opened diaphragm to avoid creation of a restriction in the flow.

d) The downstream diaphragm is an eight-petaled diaphragm opening into the circular driven tube. A circular configuration is adequate in this case because the mechanism of the opening process is such that a fully opened diaphragm is readily achieved. In general, the downstream diaphragm opens with excessive speed and, as a result, whole petals or chunks of petals can be torn off. The eight-petal arrangement has been found to alleviate this by permitting the petals to open completely without a significant amount of tearing at the hinge line.

The diaphragms discussed here have been observed to give an average efficiency of 80 to 85% for both $\frac{1}{2}$ and $\frac{5}{8}$-in. thickness over a series of shock-tunnel tests involving in the neighborhood of one hundred runs. During this period there was not a single incidence of diaphragm-petal loss and only on one occasion was a chunk of metal torn from a petal. Although the demonstrated efficiency is still less than 100%, it represents a significant improvement from the 50 to 55% that was obtained prior to the diaphragm studies discussed in this paper.

Conclusions

The effects of compressibility on driver gases composed of pure helium or helium/nitrogen mixtures have been studied analytically with the use of the virial equation of state. Second and third virial coefficients obtained from the Leonard-Jones 6–12 interaction model were used in the calculations. Driver pressures as high as 30,000 psi have been considered. Analysis shows the shock Mach number for tailored-interface operation to be increased by 0.4 to 0.6 above the ideal-gas values for a wide range of shock Mach numbers for the highest pressure studied. Experimental data show the increase to be one and one-half to two times this amount and the trends exhibited by both the real-gas analysis and the ideal-gas analysis to be correct.

It appears possible to predict shock Mach numbers for tailored operation within 10%. Furthermore, if the performance characteristics of a given facility are known at a few test conditions, the reflected pressure and enthalpy, as well as the shock Mach number for tailored operation, at any other test condition can be computed with certainty. The complete computation of the properties of the driver expansion, including real-gas effects, diaphragm opening characteristics, and finite nozzle throat diameters, appears to be necessary if the performance is to be predicted accurately.

A brief analysis of large throat to driven-tube diameter ratios was made to determine the effects of finite throat areas. It was found that a significant decrease due to throat effects existed for both stagnation pressure P_5 and enthalpy h_5. This is primarily due to a decrease in the strength of the stopping shock. When high Reynolds number and high stagnation enthalpy are required, an improvement in test duration can be achieved by preheating the driven tube and tailoring at a reduced incident shock Mach number.

An analysis of the thick-diaphragm opening process has been developed for both single and double-diaphragm installations. Both hinge moment due to plastic deformation and reduction in pressure force due to the unsteady expansion in the driver gas have been considered. A strength factor, which controls the maximum angle of petal travel during opening, has been identified. The strength factor increases with the square of diaphragm thickness and decreases linearly with pressure and the square of diameter. The fundamental problem with high-pressure diaphragms is that the thickness necessary to withstand the pressure before burst increases linearly with pressure. As a result, strength factor increases linearly as design operating pressure is increased, and it becomes progressively more difficult to obtain satisfactory opening. No relief can be obtained by increasing the tube diameter because the thickness of material required to withstand the pressure increases linearly with increasing diameter and the strength factor remains unchanged. It appears, therefore, that an upper pressure limit exists, above which simple diaphragms cannot be used satisfactorily. Petal tip velocity at impact and time required for opening have been obtained from the analysis. In addition, the performance penalties associated with diaphragm petals that do not open completely have been identified.

Experiments performed in parallel with the analysis have produced a diaphragm design which is capable of satisfactory operation at pressures up to 30,000 psi. The maximum strength factor for satisfactory operation is observed to be slightly lower than the predicted value for both upstream and downstream diaphragms; single diaphragms behave in a manner identical to downstream diaphragms. Measurements of petal tip velocity at impact and time required for opening were not obtained, although qualitive information on impact velocity was available from an inspection of petal tip condition.

In general, problems associated with high-Reynolds number operation of shock tunnels are seen to be more amenable to solution than the problems (such as shock attenuation and interface mixing) encountered in high-enthalpy operation.

References

[1] Flagg, R. P., "Detailed Analysis of Shock Tube Tailored Conditions," RAD-TM-63-64, Sept. 1963, AVCO Corp., Wilmington, Mass.

[2] Hirschfelder, J. O., Curtiss, C. F., and Bird, R. B., *Molecular Theory of Gases and Liquids*, Wiley, New York, 1954,

[3] Lewis, C. H. and Burgess, E. C., "Charts of Norman Shock Wave Properties in Imperfect Air," AEDC-TR-65-196, Sept. 1965, Arnold Engineering Development Center, Tullahoma, Tenn.

[4] Liepmann, H. W. and Roshko, A., *Elements of Gas Dynamics*, Wiley, New York, 1957,

[5] Amdur, I. and Mason, E. A., "Properties of Gases at Very High Pressures," *The Physics of Fluids*, Vol. 1, No. 5, Sept. 1959, p. 370.

[6] Norman, W. S., private communication, 1973, Arnold Engineering Development Center, Tullahoma, Tenn.

[7] Copper, J. A., Miller, H. R., Hameetman, F. J., "Correlation of Uncontaminated Test Durations in Shock Tunnels," Fourth Hypervelocity Techniques Symposium, Nov. 1965.

[8] Russel, D. A., "A Study of Area Change Near the Diaphragm of a Shock Tube. Hypersonic Research Project," Memo 57, July 1960, California Inst. of Technology, Pasadena, Calif.

[9] White, D. R., "Influence of Diaphragm Opening Time on Shock Tube Flows," *Journal of Fluid Mechanics*, Vol. 4, Pt. 6, Nov. 1958.

[10] Shigeley, J. E., *Mechanical Engineering Design*, McGraw-Hill, New York, 1963.